Arabian Journal for Science and Engineering (2024) 49:1913–1929
https://doi.org/10.1007/s13369-023-08049-4

RESEARCH ARTICLE-MECHANICAL ENGINEERING

Experimental Study on Influence of Aspect Ratio and Auxiliary Blade Profile on the Performance of H-Type Darrieus Wind Rotor

Kanthala Uma Reddy[1] · **Bachu Deb**[1] · **Bidesh Roy**[1]

Received: 11 January 2023 / Accepted: 11 June 2023 / Published online: 6 July 2023

Abstract

The performance of H-type Darrieus wind rotor (known as H-rotor) can be significantly influenced by altering its aspect ratio and incorporating an auxiliary airfoil. However, there is still a lack of comprehensive studies on the effects of these alterations. To address this gap, the present study aims to investigate the performance characteristics of H-rotors under low wind speed conditions (4–8 m/s) by using standard and auxiliary H-rotor configurations in a wind tunnel environment. A systematic analysis was conducted to examine the effect of altering the aspect ratio by changing the rotor diameter on both rotor configurations. The results of the study suggest that an aspect ratio of 1.0 provides the best performance for both standard and auxiliary H-rotors. The use of aspect ratios of 0.9 and 1.1 results in lower performance across all tested wind speeds. Moreover, the auxiliary H-rotor exhibits superior self-starting capability with a maximum static torque coefficient (C_{ts}) of 0.119, which is 80.3% higher than the maximum C_{ts} of the standard H-rotor (0.066). Additionally, the auxiliary H-rotor has a broader operating range of tip speed ratio (TSR) of 0.35–2.2 compared to the standard H-rotor TSR range of 0.4–1.9, suggesting that the auxiliary H-rotor can function dependably in diverse wind conditions. Furthermore, the auxiliary H-rotor achieves a nearly 5% increase in maximum power coefficient ($C_{p,\,max}$) compared to the standard H-rotor. The study emphasizes that the use of aspect ratio and auxiliary blades can effectively boost the efficiency of H-rotors in low wind speed conditions.

Keywords Low wind speed · NACA 0018 · Power coefficient · Tip speed ratio

1 Introduction

Wind turbines are a well-established and rapidly increasing commercial technology for sustainable development as it provides renewable, clean, and low-cost electricity [1, 2]. Generally, the official category of a wind turbine was specified by its axis orientation. They are VAWTs (Vertical axis wind turbines) and HAWTs (Horizontal axis wind turbines) [3]. The HAWTs have a lengthy history of development and modification, making them popular and reliable turbines. However, in urban and rural areas where wind speed is less predictable, VAWTs are quite appealing and well-suited for utilisation. Consequently, VAWT is an excellent alternative to lengthy HAWT for on-ground installation and mounting on buildings and rooftops. The key benefit of VAWTs is that they do not need a yawing device to counter the wind direction. Furthermore, VAWTs run at a low Tips speed ratio (TSR), resulting in reduced noise levels [4, 5].

VAWTs may feature either lift or drag-based rotors. The most common drag-based VAWT is the Savonius rotor, and have a low C_p and good self-starting [5–7]. In contrast, the Darrieus rotor is the dominant lift-based model of VAWT and comparatively had higher C_p and poor starting characteristics [8–10].

A significant amount of research has been conducted, including wind tunnel experiments and numerical simulation, to evaluate and enhance the starting torque and power performance of Darrieus rotors [11–15]. In particular, Sengupta et al. [11] used the centrifugal blower test rig to test three different blade profiles at low wind speeds. The findings demonstrated that, compared to an H-rotor with NACA 0018 and EN0005 blades, S815 bladed H-rotor had more significant C_{ts} and superior C_p values. The impact of aspect

---

✉ Kanthala Uma Reddy
kanthala.umareddy@gmail.com

Bachu Deb
bdebnitmz@gmail.com

[1] Department of Mechanical Engineering, National Institute of Technology Mizoram, Aizawl 796012, India

ratio on H-rotor performance was examined by Li et al. [16] using a panel analysis method. The findings indicate that the efficiency of an H-rotor is highly dependent on its aspect ratio. Moreover, it suggests that adequately managing the aspect ratio helps reduce fluid flow curl, which increases the amount of energy harvested from the wind. Studies of H-rotors [17–20] have used the parameter "solidity" which depends on both the aspect ratio and the number of blades, to great effect. They have shown that a rotor with more solidity results in a lower TSR for the maximum power coefficient. They also concluded that the parameter aspect ratio, along with solidity, is a critical feature in rotor operating conditions, specifically for small-scale wind turbines [8, 21–23]. Nguyen et al. [24] performed a numerical assessment of the influence of blade thickness on starting torque at different rotational orientations for an H-rotor operating at 3–7 m/s wind speed using data from four depleting blades (NACA 0012, 0015, 0018, and 0021). They found that the static torque increased linearly with airfoil thickness. Ghiasi et al.[21] analysed the performance of H-rotors with varying chord lengths at three levels: 0.1, 0.15, and 0.2 m; varying blade numbers: 2, 3, and 4 blades; varying aspect ratios of 0.5–2; and four types of airfoils: NACA 4418, 4412, 0018, and 0012. Simulations were conducted at low Re ($Re < 10^5$) and four TSRs: 1, 2, 3, and 4. Wind turbines operate better at low TSRs when the H-rotor has more blades, extended chords, and a larger aspect ratio. However, this pattern overturns at high TSRs. Furthermore, among the four examined kinds of airfoils, the NACA 4412 airfoils had the best performance at TSR 1–3. Parker and Leftwich [25] examined the H-rotor performance concerning the influence of the TSR. From the outcomes, it was understood that, as TSR increased, the progressive regularity of the vortex detaching increased in comparison to the freestream. Jain and Saha [26] used numerical modelling to examine the impact of the blade t/c (thickness to chord) ratio on the presence of the dynamic stall in an H-rotor. The results showed that a t/c ratio of 9% yields the maximum C_l (lift coefficient), while a t/c ratio of 12% optimises the static torque behaviour of the H-rotor.

H-rotor performance has been improved through the widespread application of passive control techniques on rotor layout in recent years. Passive control devices mounted on the H-rotor blades have been shown to improve starting capability and power efficiency by preventing or greatly minimising the occurrence of negative torque development under low TSR situations. Most commonly used passive control methods include: incorporating tubercles on the leading edge (LE) of the airfoil [27], using dimple [28], implementing of gurney flap (GF) [29, 30], using slat airfoils [9], applying wind lens [31] and wind deflectors [32]. 2D numerical simulation with a dimple on the airfoil was carried out by authors [28, 33] and suggested that implementing the cavity on the pressure side could expand the torque generation of the rotor at all TSR ranges. Nevertheless, in low wind speed circumstances, the presence of the cavity on the suction side of the airfoil has no discernible impact. Conversely, using a cavity on the blade might lessen its rotating stiffness. Therefore, the implementation of the dimple is insignificant to avoid structural failure of the rotor blade. Zidane et al.[32] performed a 2D numerical simulation to optimize the H-rotor performance both with and without the wind deflector. The results show that at low TSR, the deflector impact is little on torque and power of the H-rotor. Studies [34–36] on GF application on H-rotor indicate that the GF can relegate the flow separation across the rotor blades. However, GF implementation involves more noise generation and an increment in drag generation. Moreover, some studies [5, 36] found that the GF could not enhance the C_p at high TSR. Wang and Zhuang [37] observed that the LE serration could develop the maximum lift coefficient of the blades up to 25% more than the clean airfoil and no significant improvement in the drag coefficient. However, some studies by [38–40] observed that a high TSR value leading-edge serration leads to more negative torque creation as they presented giant vortices at blade wake compared to the clean rotor. This result indicates that LE serration does not significantly affect the performance of the H-rotor. Arpino et al. [7] recommended employing the utilisation of an H-rotor equipped with additional blades. The numerical results demonstrate that even though the wind speed was only 3 m/s, the intended H-rotor with extra blades is still able to reach a C_p value of 0.10 and a rated C_t value of 0.07. Both C_p and C_t were investigated throughout a TSR range of 1–2, with the highest value for dynamic power being 0.18 at $TSR = 1.5$ and the lowest value for C_t being 0.13 at $TSR = 1.2$. It has been established that this type of design is appropriate for use in very light wind conditions. Zamani et al. [41] analysed a new Darrieus rotor with a J-shaped airfoil using simulations. They found that the J-shaped airfoil significantly improved self-starting by increasing the starting torque, which enhanced the overall performance of the rotor. The use of the J-shaped profile also reduced vibration and fatigue stress by decreasing the torque amplitude, achieved through a narrower profile width. Chen et al. [42] recommended a new design of the rotor blade profile by implementing the opening on the airfoil pressure of the suction side. Their outcomes have revealed that opening an airfoil can augment the torque generation at a lower TSR range and low wind speed condition. However, the improved torque was not maintained at higher TSR ranges.

CFD investigations that are validated can be a powerful tool for wind turbine optimization and characterization. However, experiments are still necessary to supplement CFD studies. Wind tunnel experiments were conducted on H-rotors in studies and revealed that conducting field studies can be challenging due to varying local weather conditions

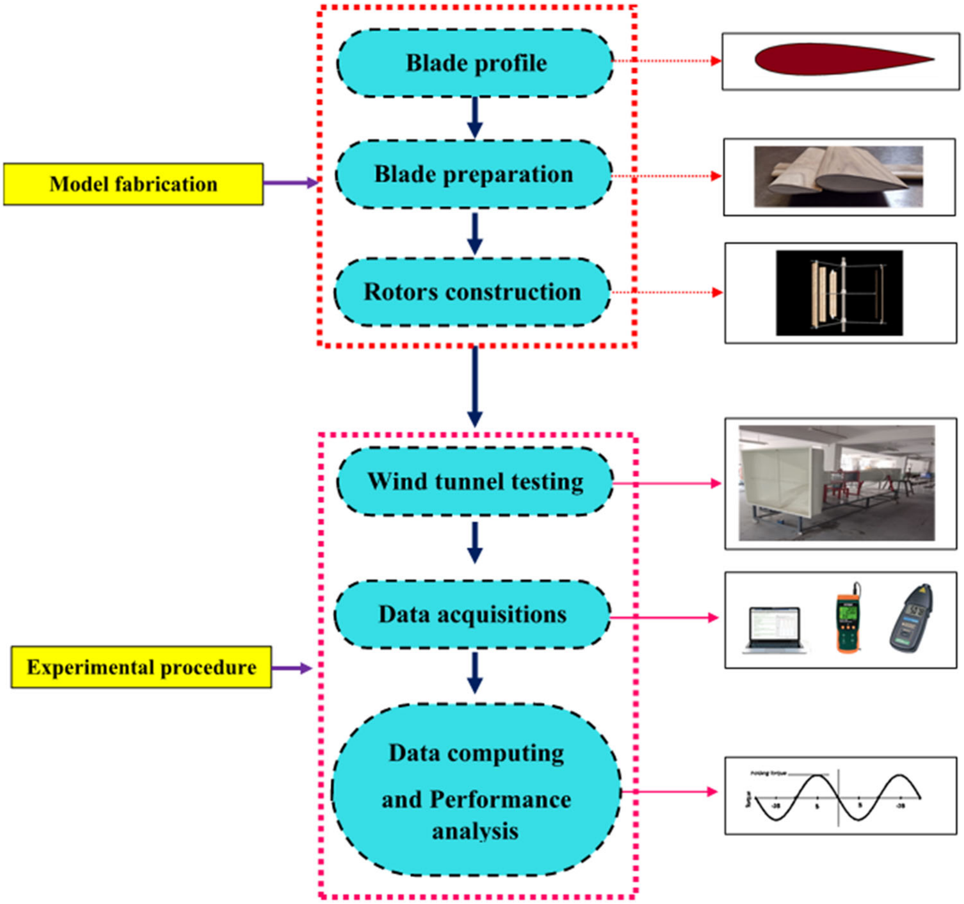

Fig. 1 Flow chart of model fabrication and experimental procedure

and wind speeds. In such cases, wind tunnel testing is essential to maintain a consistent testing environment. Li et al. [43] conducted wind tunnel tests on dual VAWTs with different rotor spacing as well as isolated VAWTs. The results indicated that the impact of the dual VAWT design on overall power production was minimal when compared to isolated VAWTs. Scungio et al. [44] performed experimental work on an innovative Darrieus-style rotor with auxiliary blades. The results demonstrated that the innovative rotor had high starting characteristics but low power performance compared to the traditional straight-bladed Darrieus rotor.

Implementing auxiliary airfoils in lift-type VAWT neither falls in the passive control technique nor the multi-element airfoil. Mostly, in passive control techniques and multi-element airfoil usages, the airfoil model will have undergone attachment or detachment of one portion or segment to change the flow direction. In an auxiliary airfoil case, there are two airfoils (called main and auxiliary airfoil), the airfoil outlines not be modified, and an extra supplementary airfoil with a different chord length could be used at behand the main airfoil.

Despite the extensive research conducted on airfoil optimization, blade thickness ratio, and solidity, specific studies on auxiliary airfoils and altering aspect ratio remain limited. As such, this study seeks to address this gap in the literature and provide a comprehensive investigation into the performance of H- rotors with varying aspect ratios and auxiliary blade profiles. Furthermore, this study provides precise and detailed data on the performance of both standard and auxiliary H-rotors across various aspect ratios and low wind speeds, making significant contributions to the field. The results emphasize the crucial role of aspect ratio and auxiliary blade profiles in improving H-rotor performance in terms of static and dynamic torque as well as power coefficients. These findings are particularly valuable to researchers and engineers in the wind energy sector as they enhance the understanding of the factors influencing H-rotor performance.

2 Construction of H-rotor Models and Experimental Method

The present section discusses the construction of H-rotor models along with the procedure of wind tunnel experimentation and data measuring techniques. Figure 1 illustrates the system of approaches for model fabrication and experimental procedure.

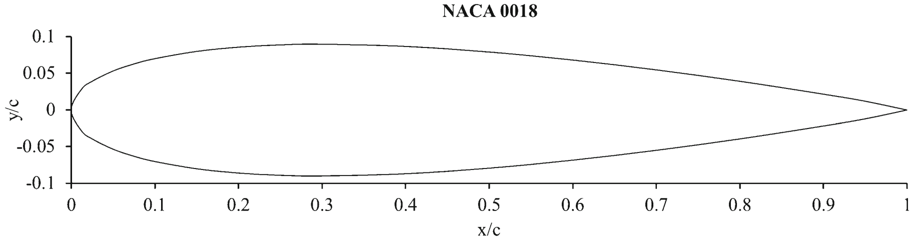

Fig. 2 Outline of NACA 0018 airfoil


a)
b)

Fig. 3 Fabricated H-rotors **a** standard H-rotor **b** auxiliary H-rotor

2.1 selection of Blade Profile

The construction of the model began with the selection of appropriate blade profiles. According to a review of the relevant literature [19, 39, 45–48], NACA series blade profiles are widely utilised and acknowledged as among the most effective turbine blades. The present investigation selected the NACA 00XX series airfoil for rotor blades, i.e., NACA 0018 can be seen in Fig. 2.

2.2 Blade Preparation and Rotors Construction

The modelled turbines are standard H- rotors and auxiliary H-rotors consisting of symmetrical NACA 0018 blades (t/c is 18%), the best airfoil in the NACA symmetrical series [9, 49]. Primarily the outline of a symmetrical NACA 0018 airfoil shape was generated, shown in Fig. 2. Later, the procedure outlined by the authors [11, 50–52] is utilised to create the rotor blades. Because of its excellent strength-to-weight ratio, portability, and rigidity in the face of high winds, Balsa wood is ultimately selected as the blade material [53].

Table 1 Specification of H-rotors

Specification	Rotors	
	Standard H-rotor	Auxiliary H-rotor
Main airfoil	NACA 0018	NACA 0018
Auxiliary airfoil	–	NACA 0018
Main blade Chord length (C_1)	100 mm	100 mm
Auxiliary blade Chord length (C_2)	–	50 mm
Height of the blades (H)	300 mm	300 mm
Dia. of the rotors (D)	330 mm, 300 mm, 270 mm	330 mm, 300 mm, 270 mm
Aspect ratio	0.9, 1.0 and 1.1	0.9, 1.0 and 1.1
Longitudinal separation (S_l)	–	40 mm
Radial separation (S_r)	–	30 mm

The fabricated models of standard and auxiliary H-rotor are shown in Fig. 3a, b. The dimensions of the tested rotors can be seen in Table 1. Figure 4 depicts a 2D schematic representation of the auxiliary H-rotor. The auxiliary H-rotor is composed of three pairs of blade profiles, each consisting of a main and an auxiliary blade. Figure 5a displays the geometrical features of the main and auxiliary airfoil arrangement, while Fig. 5b shows the blade specification of the standard H-rotor. The main blades have a height (H) of 30 cm and chord (C_1) of 10 cm, while the auxiliary blades have a height of 30 cm and chord (C_2) of 5 cm, maintaining a C_2/C_1 ratio of 0.5. According to Scungio et al. [44] and Uma Reddy et al. [54] the longitudinal separation (S_l) for auxiliary H-rotor systems typically ranges around 40% of the chord length of the main airfoil, while the radial separation (S_r) typically ranges around 30% of the chord length of the main airfoil. Therefore, in this study, S_l is maintained equal to 0.4 × C_l and S_r

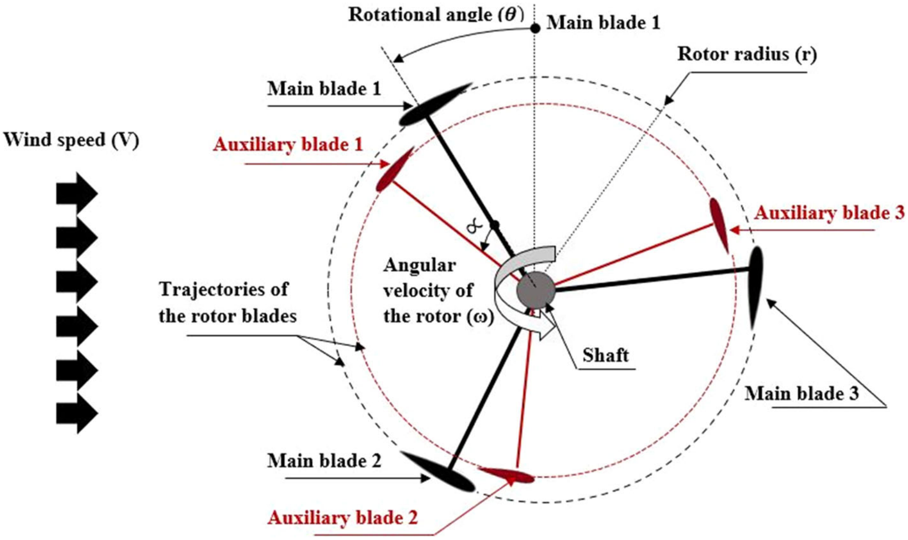

Fig. 4 Schematic view of the auxiliary H-rotor

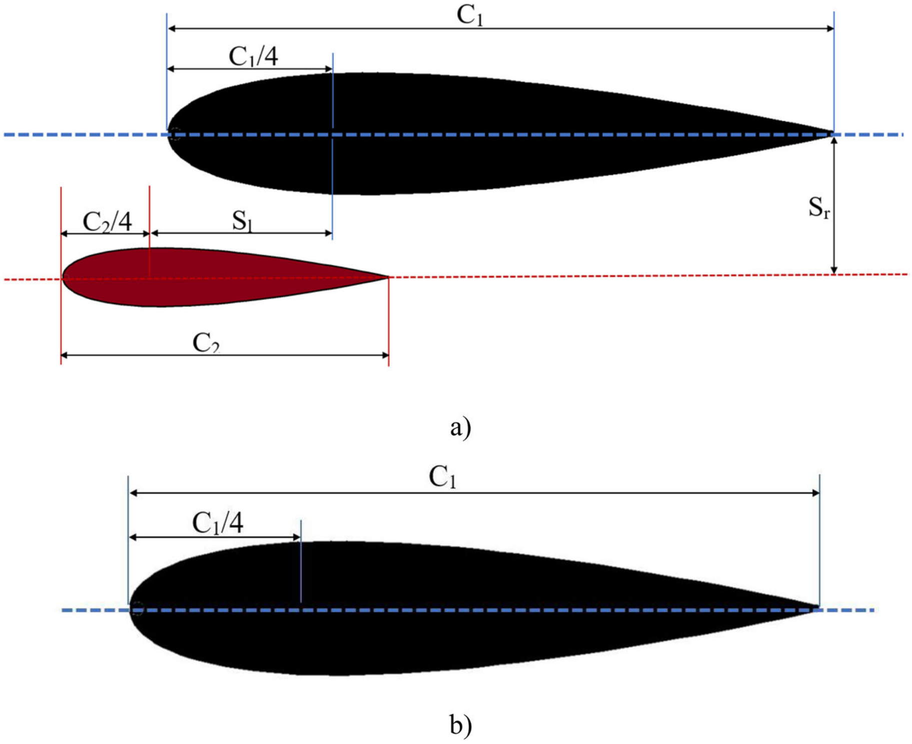

Fig. 5 Blade profiles **a** main and auxiliary airfoil **b** main airfoil

equal to $0.3 \times C_1$, consistent with these typical values. These blades are coupled to a mild steel shaft radius of 0.6 cm and length of 70 cm with the aid of threaded round struts. Two struts are used for placing each blade at the bottom and top locations. The rods were 20 cm long, 4 mm in radius, and spaced 120° away from one another before being arc-welded to the center shaft. For arranging auxiliary blades into the rotor, the holes are created at the midpoint of the auxiliary blades and fixed to the rotor shaft. The dimension between the main and auxiliary blades was measured and adjusted with the help of Vernier calliper and bolt and nut arrangements. The bolt and nut assembly are used to adjust the diameter, consequently, aspect ratio (H/D) of the H-rotors, which is defined as the ratio of Height of the rotor blade (H) to diameter of the rotor (D). Regarding auxiliary H-rotor, it should be noted that the auxiliary airfoil is an additional airfoil that does not significantly alter the fundamental measuring parameters of the rotor, such as the diameter of the rotor, chord length of main airfoils, shaft diameter, and aspect ratio. Therefore, these parameters remain very similar to those of the standard H-rotor.

Fig. 6 Experimental test rig **a** sub-sonic wind tunnel **b** rotor setup

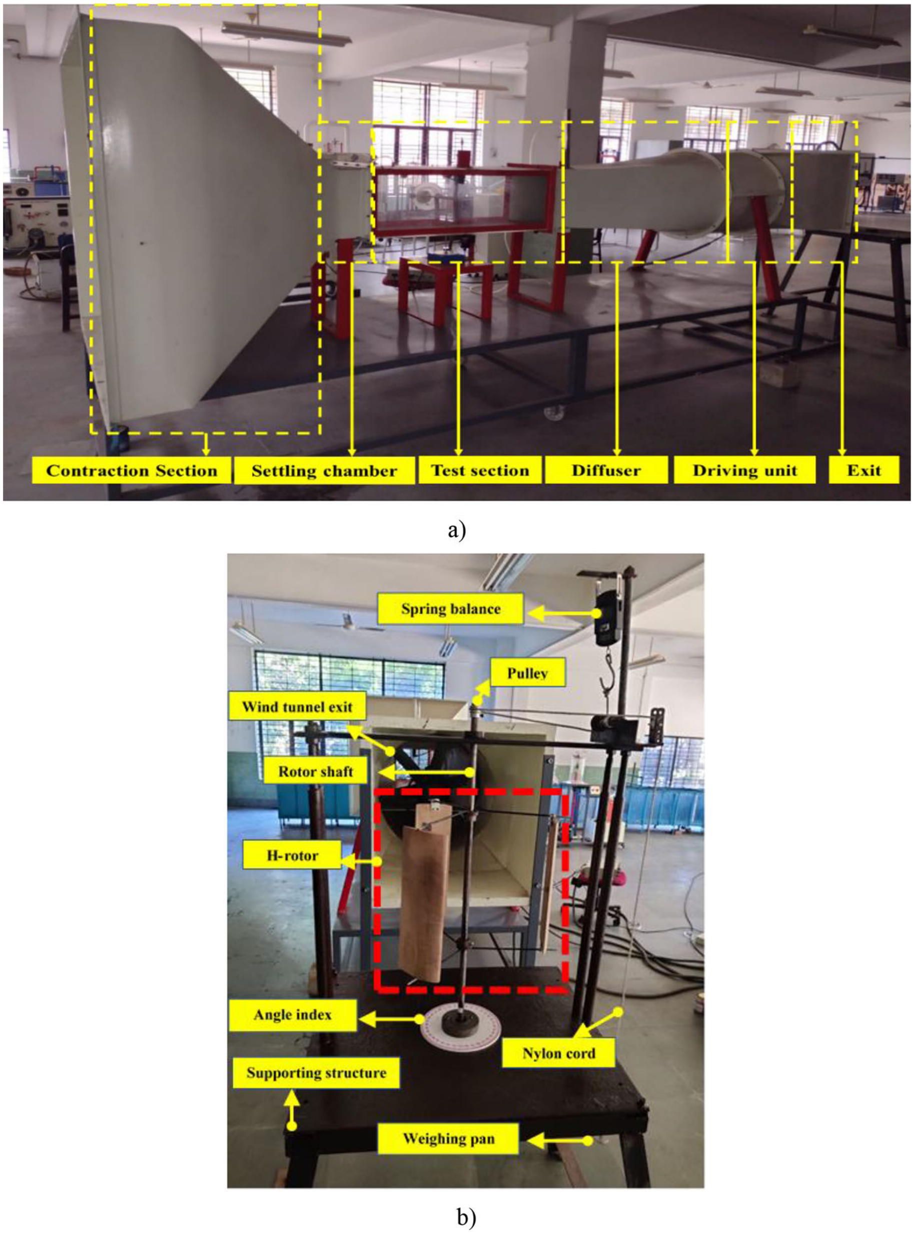

2.3 Wind Tunnel Testing

The experiments were conducted in an Eiffel-type subsonic wind tunnel consisting of a contraction section, settling chamber, test section, diffuser, and driving unit, as shown in Fig. 6a. For laboratory-level investigations of VAWT, the size of the measurement section of the wind tunnel determines whether experimental investigations will occur within the test section or at the exit section. As depicted in Fig. 6b, the H-rotors under testing were held vertically within a steel housing, which was positioned at the wind tunnel's exit. Two ball bearings, one at each end of the supportive structure to which the H-rotors were attached, kept them aligned along their central axis or shaft. The bearings were periodically oiled to prevent friction. The H-rotors were installed 150 cm past the subsonic wind tunnel's outflow, with their vertical axis of rotation being equal to the centreline of the turbine.

The tested models are exclusively laboratory scaled models; however, the obtained results can be extended to full size turbine by maintaining the geometric similarity between the scaled model (SM) and the full-size (FS) turbine. This means that the size and shape of the components in the model should be proportional to those in the full-size turbine, as shown in Eq. (1), which includes the height of the turbine blade (H) and the turbine diameter (D) [55].

$$\frac{H_{SM}}{H_{FS}} = \frac{D_{SM}}{D_{FS}} \tag{1}$$

Besides maintaining geometric similarity, there are other factors that need to be considered when extrapolating experimental results from scaled models to full-sized wind turbines. These factors include the Reynolds number, the tip-speed ratio, and the aspect ratio. It is critical to match these parameters between the scaled model and the full-sized turbine to ensure that the outcomes accurately represent the behaviour of the full-sized turbine.

2.4 Instrumentation and Data Measurement

The H-rotors were allowed to spin from a zero-load condition, and a digital tachometer was used to determine the rotational speed (ω) once the rotor reached a uniform condition. A Extech SDL 350 Hot wire anemometer and data logger were used to measure the wind speed at different locations in front of the H-rotor, and average wind speed values were considered as the free stream wind speed. Due to varying atmospheric pressure conditions and inflow conditions, it is challenging to obtain the exact desired wind speed, and the measured and calculated averaged wind speed was 4.05 m/s, 6.11 m/s, and 8.1 m/s, with wind speed uncertainty considered in the performance calculation of H-rotors. The rotors were gradually loaded with 50 g mass increments from dead load to the extremity load that makes the rotor stationary, and the mechanical force applied to the rotating shaft and the rotational speed at various wind speed values were recorded to calculate the mechanical brake power of the tested H-rotors. The setup used for this is shown in Fig. 6b and consists of a weighing pan, nylon string, pulley system, and spring balance. The spring balance index and weighing pan are connected with a nylon thread of 1 mm radius, as shown in Fig. 6b. The following Eq. (2) is used to determine the braking torque (t) [11, 50, 51].

$$t = (w_a - s_{bi}) \times (0.5 \times (d_p + d_c)) \times g \tag{2}$$

here w$_a$ is applied weight in Kg, S_{bi} is the spring balance index, d_p is the diameter of the pulley, and d_c is the diameter of the cord.

The mechanical power can be computed using the rotational speed and mechanical torque measurements as shown in Eq. (3).

$$P = t \times \omega \tag{3}$$

Static torque coefficient (C_{ts}) [54]

$$C_{ts} = \frac{ts}{0.5\rho U_f^2 Ar} \tag{4}$$

Dynamic torque coefficient (C_t) [54]

$$C_t = \frac{t}{0.5\rho U_f^2 Ar} \tag{5}$$

Power coefficient (C_p) [54]

$$C_p = \frac{p}{0.5\rho U_f^3 A} \tag{6}$$

The tip speed ratio (λ) [55]

$$\lambda = \frac{D\omega}{2U_f} \tag{7}$$

here ts, t, U_f, A, and r, are representing static torque, dynamic torque, wind speed, swept area of the rotor and radius of the rotor, respectively.

3 Uncertainty Analysis and Blockage Factor

"Uncertainty in measurements" describes the inaccuracy that may be present in a measured quantity. Several factors can contribute to this uncertainty, including limitations in the measuring instrument, fluctuations in environmental conditions, or errors in the measurement technique. A widely utilized approach for determining the uncertainty associated with a measured quantity is through the use of the propagation of uncertainty formula, as demonstrated in Eq. (8). [54]

$$\delta_q = \sqrt{\left[\left(\frac{\partial q}{\partial x_1}\delta_1\right)^2 + \left(\frac{\partial q}{\partial x_2}\delta_2\right)^2 + \cdots + \left(\frac{\partial q}{\partial x_n}\delta_n\right)^2\right]} \tag{8}$$

where δ_q is the total uncertainty of the derived quantity, q (function of $x_1, x_2, \ldots, x_n$), and $\delta_1, \delta_2, \ldots, \delta_n$ are the individual uncertainties of measured variables $x_1, x_2, \ldots, x_n$.

Equation (9) shows that the measured variables are combined in a product form to obtain the derived quantity, allowing the uncertainty to be expressed as a fractional uncertainty. Therefore, Eq. 8 can be restated as Eq. (10).[54]

$$q = x_1^{a1} \cdot x_2^{a2} \cdot \cdots \cdot x_n^{an} \tag{9}$$

$$\frac{\delta_q}{q} = \sqrt{\left[\left(a_1\frac{\delta_1}{x_1}\right)^2 + \left(a_2\frac{\delta_2}{x_2}\right)^2 + \cdots + \left(a_n\frac{\delta_n}{x_n}\right)^2\right]} \tag{10}$$

where $a_1, a_2, \ldots, a_n$ are the degree of measured variables of $x_1, x_2, \ldots, x_n$

Table 2 Standard uncertainty values of the variables

Variable	U$_f$ (%)	Λ (%)	C_{ts} (%)	C_t (%)	C_p (%)
Standard uncertainty	1	1.4	2.8	2.8	3.5

The overall uncertainties (δ_o) related with both the tachometer (δ_{tm}) and anemometer ((δ_{am}) has been determined using Eq. (11).

$$\delta_o = \sqrt{\left[\left(\delta_{am}^2\right) + \left(\delta_{tm}^2\right)\right]} \tag{11}$$

Uncertainty presented in the measured data in C$_t$, C$_p$, and T can be calculated using Eqs. (12 and 13)

$$\frac{\delta C_t}{t} = \sqrt{\left(\frac{\delta t}{t}\right)^2 + \left(2\frac{\delta U_f}{U_f}\right)^2} \tag{12}$$

$$\frac{\delta C_p}{p} = \sqrt{\left(\frac{\delta p}{p}\right)^2 + \left(3\frac{\delta U_f}{U_f}\right)^2 + \left(\frac{\delta \omega}{\omega}\right)^2} \tag{13}$$

The calculation of the uncertainty related to the measurement of torque (δt) is calculated usinf Eq. (14). This calculation takes into account the least count of the spring balance (δs = 1 kg/cm^2).

$$\frac{\delta t}{t} = \frac{\delta s}{s} \tag{14}$$

The standard uncertainty values for wind speed (δU$_f$), angular rotation (δω), and spring balance (δs), are equal to 0.01 × U$_f$, 0.01 × ω, and 0.01 × S_{bi}. Finally, the standard uncertainty of all the variables is reported in Table 2.

The blockage ratio is not considered in this experiment since the experiment is performed outside the wind tunnel test section, where the blockage is minimal [56].

4 Results and Discussion

The section describes the findings pertaining to the dimensionless performance metrics (C$_{ts}$, C$_t$, and C$_p$) of the tested H-rotors. All experimental results presented here have been subjected to uncertainty adjustments. The C$_p$ and C$_t$ are calculated to the corresponding TSR. The different TSR values are obtained through break dynamometer load conditions. In contrast, the C$_{ts}$ are observed for different rotational angles (θ = 0–360° in every 30°) concerning incoming wind direction.

Fig. 7 Coefficient of Static torque (C$_{ts}$) Vs rotational angle (θ) of the H-rotors with various aspect ratios and at three wind speeds

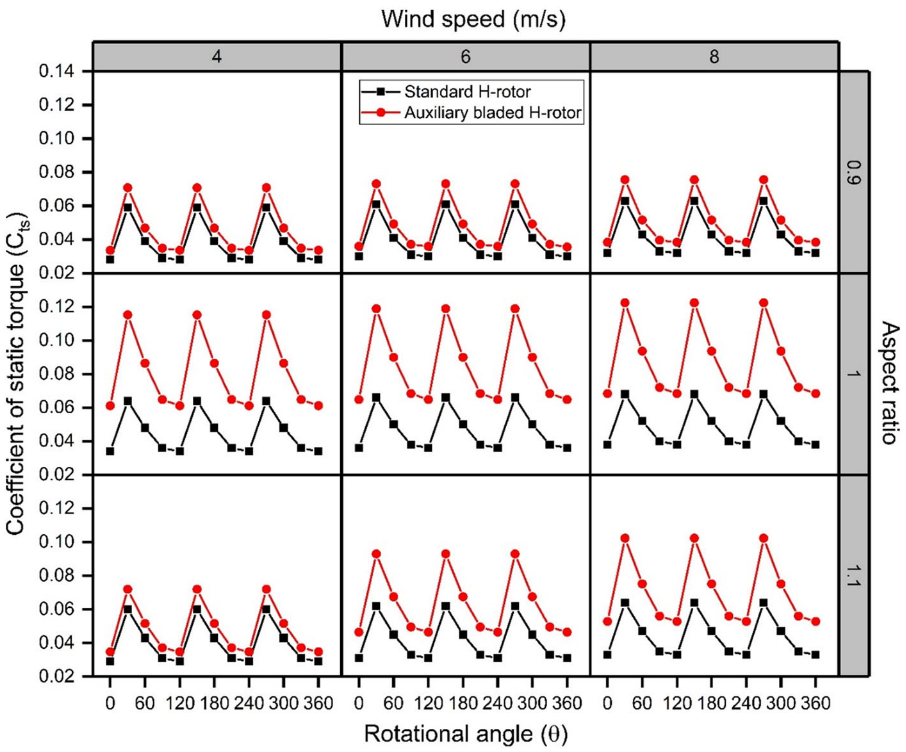

Table 3 Maximum C_{ts} values of the standard and auxiliary H-rotors

Aspect ratio	Wind speed in m/s	Standard H-rotor	Auxiliary H-rotor	% of variation
0.9	4	0.059	0.071	20.3
	6	0.061	0.073	19.6
	8	0.063	0.077	22.2
1.0	4	0.064	0.115	79.6
	6	0.066	0.119	80.3
	8	0.068	0.122	79.4
1.1	4	0.060	0.072	20.0
	6	0.063	0.093	32.2
	8	0.067	0.102	52.2

4.1 Static Torque Performance

The trellis plots (Fig. 7) portray that the variation of C_{ts} w.r.t rotational angle (θ) for various aspect ratios (0.9, 1.0 and 1.1) and wind speeds (4 m/s, 6 m/s and 8 m/s) in order to understand the distribution of C_{ts} at various angles of the H-rotors in the complete rotational cycle. The rotational angle of the rotors is measured with the aid of an angle indexing disc; for every 30°, the C_{ts} is calculated using Eq. (4). From the Fig. 7, it can observe that the C_{ts} value is increased from 0° to 30° then after 30° to 90° the C_{ts} value is decreased, from 90° to 120° there is a very slight change in C_{ts} value. The standard and auxiliary H-rotors both exhibited the same trend, with the exception of a shift in the coefficient value. The maximum C_{ts} value is obtained at 30°, and from there, the maximum values are repeated every 120° since a typical three-bladed H-rotor has the same line patterns for every 120°. It can observe from Fig. 7 that the C_{ts} values for the auxiliary H-rotor are substantially more significant at every combination of aspect ratio and applied wind speed than those for the standard H-rotors.

The C_{ts} values of standard and auxiliary H-rotors with an aspect ratio of 1.0 are found to be greater than those with 0.9 and 1.1. The highest C_{ts} were equivalent to 0.064, 0.066, and 0.068 for the standard H-rotor (aspect ratio 1.0) when the wind speed was 4 m/s, 6 m/s, and 8 m/s, respectively. While the highest C_{ts} value of the auxiliary H-rotor (aspect ratio 1.0) is equivalent to 0.115, 0.119, and 0.122, corresponding to approximately 79.6%, 80.3%, and 79.4% of the increment, respectively. Table 3 represents the maximum C_{ts} values of the standard and auxiliary H-rotors with three aspect ratios and wind speeds. Further, the average C_{ts} values of the standard and auxiliary H-rotor is calculated as shown in Fig. 8 where both the rotors have positive C_{ts} values. A further observation that can be made from Fig. 8 is that the C_{ts} values of both the standard and auxiliary H-rotors increases as the wind speed increases. Furthermore, the results depicted in Fig. 8 indicate that when comparing aspect ratios of 0.9 and 1.1 to an aspect ratio of 1.0, consistently higher average C_{ts} values are obtained for both rotors at all tested wind speeds. This suggests that maintaining an aspect ratio of 1.0 is advantageous in terms of achieving higher C_{ts} values. Specifically, at an aspect ratio of 0.9, the standard H-rotor exhibits a maximum average C_{ts} value of 0.042 at 8 m/s, while the auxiliary H-rotor exhibits a maximum average C_{ts} value of 0.05 at the same wind speed. In contrast, at an aspect ratio of 1.0, the standard H-rotor exhibits a maximum average C_{ts} value of 0.049 at 8 m/s while, the auxiliary H-rotor demonstrates a maximum average C_{ts} value of 0.087 at the same wind speed. Similarly, at an aspect ratio of 1.1, the standard H-rotor and the auxiliary H-rotor exhibit maximum average C_{ts} values of 0.044 and 0.07, respectively, at 8 m/s. These findings suggest that maintaining an aspect ratio of 1.0 is the optimal choice for maximizing the average C_{ts} values of the H-rotors.

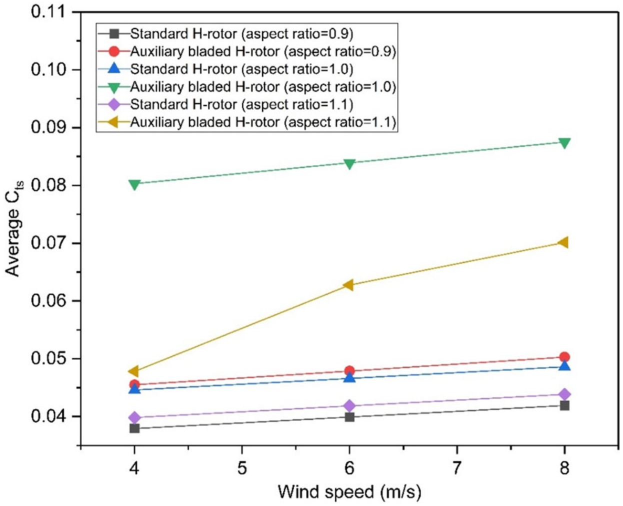

Fig. 8 Average coefficient of static torque of the rotors

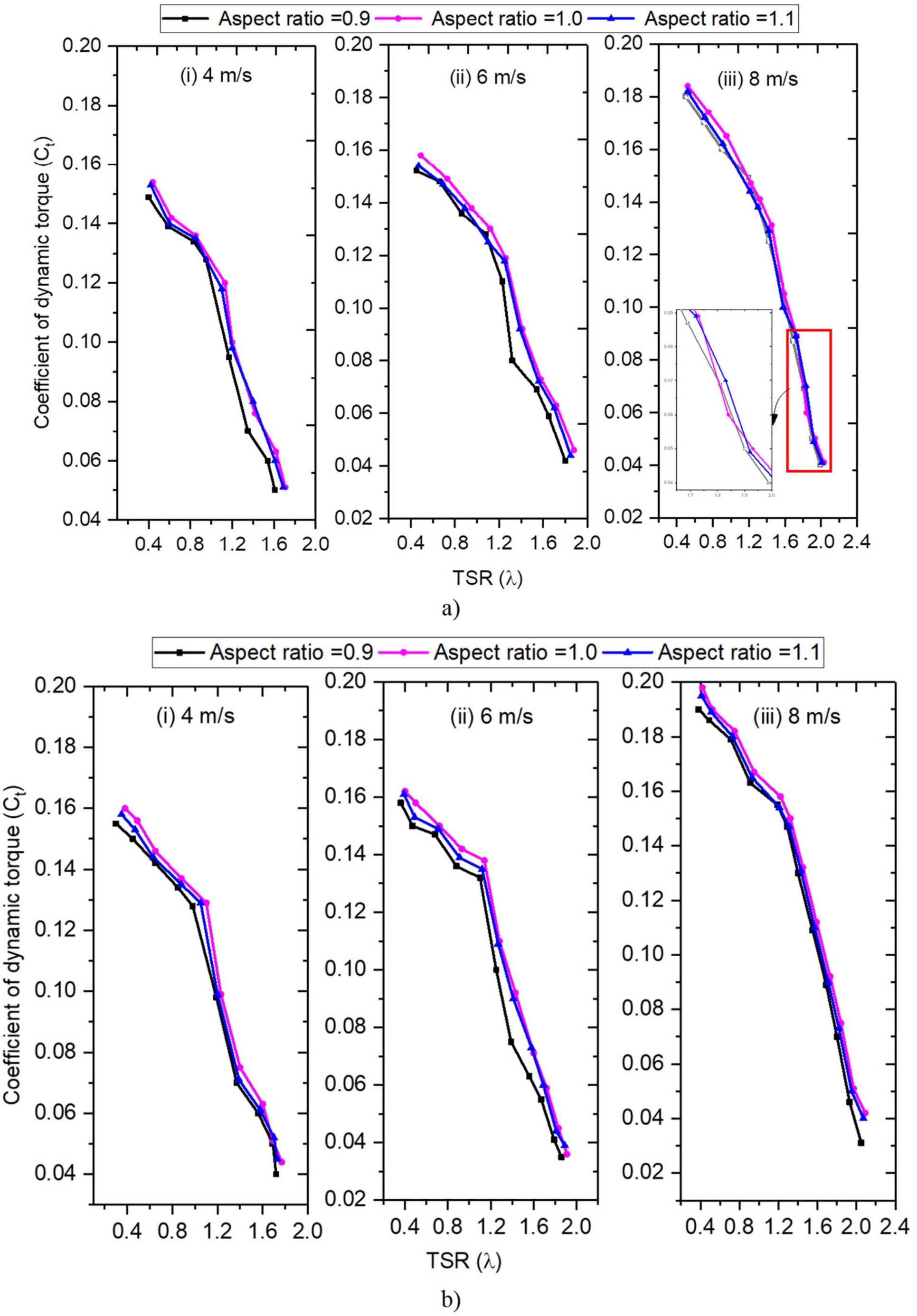

Fig. 9 Variation of dynamic torque (C_t) at various wind speeds **a** standard H-rotor **b** auxiliary H-rotor

4.2 Dynamic Torque Variation

In Fig. 9, the results indicate the variation of C_t with respect to TSR, where C_t is calculated using Eq. (5). The C_t values for the standard and auxiliary H-rotors are found to be inversely proportional to TSR, decreasing linearly as a function of TSR. The TSR working range for a standard H-rotor is 0.4–1.9, whereas for an auxiliary H-rotor it is 0.35–2.2. This indicates that in the TSR range of 0.35–0.4, the standard H-rotor produces substantially zero torque, resulting in zero output power. This low TSR working feature is a considerable advantage of the auxiliary H-rotor.

In Fig. 9a, it can be seen that the C_t values of the standard H-rotor reach a maximum of 0.154 at a TSR of 0.44 for an aspect ratio of 1.0 and a wind speed of 4 m/s. However, the auxiliary H-rotor at the same aspect ratio and wind speed produces higher C_t values of 0.16 at a lower TSR of 0.38, as

Table 4 Maximum, average, and minimum coefficient of dynamic torque (C_t) of the standard and auxiliary H-rotors at various wind speeds

Wind speed (in m/s)	Aspect ratio	Standard H-rotor			Auxiliary H-rotor		
		$C_{t, max}$	$C_{t, avg}$	$C_{t, min}$	$C_{t, max}$	$C_{t, avg}$	$C_{t, min}$
4	0.9	0.149	0.1035	0.050	0.155	0.1027	0.041
	1.0	0.154	0.1045	0.051	0.160	0.1060	0.044
	1.1	0.153	0.1038	0.051	0.158	0.1047	0.045
6	0.9	0.152	0.1026	0.042	0.158	0.099	0.035
	1.0	0.158	0.1075	0.048	0.162	0.1057	0.036
	1.1	0.154	0.1057	0.044	0.161	0.1047	0.039
8	0.9	0.180	0.1160	0.040	0.190	0.1245	0.031
	1.0	0.184	0.1170	0.041	0.198	0.1290	0.042
	1.1	0.182	0.1160	0.041	0.195	0.1270	0.040

shown in Fig. 9b. Similarly, at wind speeds of 6 m/s and 8 m/s, the auxiliary H-rotor demonstrates higher C_t values, with 0.162 at TSR = 0.4 (6 m/s) and 0.198 at TSR = 0.42 (8 m/s), compared to the standard H-rotor which only achieves 0.158 at TSR = 0.49 (6 m/s) and 0.184 at TSR = 0.52 (8 m/s).

The maximum, minimum, and average C_t values of the rotors are shown in Table 4. Specifically, at an aspect ratio of 0.9 with a wind speed of 4 m/s, the maximum, minimum, and average C_t values for the standard H-rotor were 0.149, 0.050, and 0.104, respectively, while the corresponding values for the auxiliary H-rotor were 0.155, 0.040, and 0.1027. This shows a 4% increase in C_t for the auxiliary H-rotor compared to the standard H-rotor at this aspect ratio. Similarly, at an aspect ratio of 1.0 and a wind speed of 4 m/s, the maximum, minimum, and average C_t values for the standard H-rotor were 0.154, 0.051, and 0.105, respectively, while for the auxiliary H-rotor, the corresponding values were 0.160, 0.044, and 0.1060, resulting in a 3.8% increase in C_t for the auxiliary H-rotor. At an aspect ratio of 1.1 and a wind speed of 4 m/s, the maximum, minimum, and average output coefficient dynamic torque of the standard H-rotor were 0.153, 0.051, and 0.104, respectively, while the corresponding values for the auxiliary H-rotor were 0.158, 0.045, and 0.1047, indicating a 3.2% increase in C_t for the auxiliary H-rotor. The results obtained at wind speeds of 6 and 8 m/s show that the auxiliary H-rotor is more efficient, with an increase of nearly 5%. The results indicate that the TSR working range improves as the wind speed increases. Additionally, auxiliary H-rotors can produce torque over a significantly wider range of TSRs than standard H-rotors. Thus, in low wind speed conditions, the auxiliary H-rotor tends to outperform the standard H-rotor in terms of C_t.

4.3 Coefficient of Power Performance

The C_p surface plot of the standard and auxiliary H-rotors against aspect ratio and TSR at varying wind speeds is shown in Figs. 10 and 11, respectively. where C_p is calculated using Eq. (6). It can observe from Figs. 10 and 11 that the TSR operating range of the standard H-rotor lies between 0.4 and 1.9, whereas, for the auxiliary H-rotor, the TSR range lies between 0.35 and 2.2. A broad TSR range means the auxiliary H-rotor can perform reliably in a variety of situations. It can also observe that as TSR increases, the C_p increases up to a specific range; in the further increment of TSR value, the C_p value decreases, which signifies the C_p values are minimal at lower and higher TSR values. Because lower TSR values were obtained at minimum load conditions (for both rotors), where the rotors spin too quickly, potentially producing too much turbulent air that acts as a solid barrier against the wind, higher TSR values were obtained at maximum load conditions, where the rotors spin very slowly, allowing a lot of wind to pass through the space between the blades instead of supplying energy to the rotor. Thus, low and high TSR values are characterized by relatively low C_p values.

The C_p surface plot of the standard and auxiliary H-rotor with three different aspect ratios operated at 4 m/s input wind speed is shown in Figs. 10a and 11a, respectively. It can observe from Fig. 10a (legend of the surface plot) the C_p of the standard H-rotor reached 0.1356, whereas, at the same wind speed, the C_p of the auxiliary H-rotor reached 0.142 (Fig. 11a), which is about 4.5% higher than that of the standard H-rotor. Likewise, the legend of the surface plot shows the maximum C_p value of the standard H-rotor (Fig. 10b, c) and the auxiliary H-rotor (Fig. 11b, c) at each wind speed. However, the maximum C_p values shown in the legend belong to rotors with an aspect ratio of 1.0 as the maximum C_p obtained for aspect ratio 1.0 for both rotors at every applied wind speed.

Among the considered wind speeds, it has been observed that at higher wind speeds (8 m/s), altering the aspect ratio from 0.9 to 1.0 results in an increase in C_p up to 5% for the standard H-rotor and 4.5% for the auxiliary H-rotor. Conversely, altering the aspect ratio from 1.0 to 1.1 results in a

Fig. 10 Coefficient power (C_p) variation of Standard H-rotor with various aspect ratio at various wind speeds

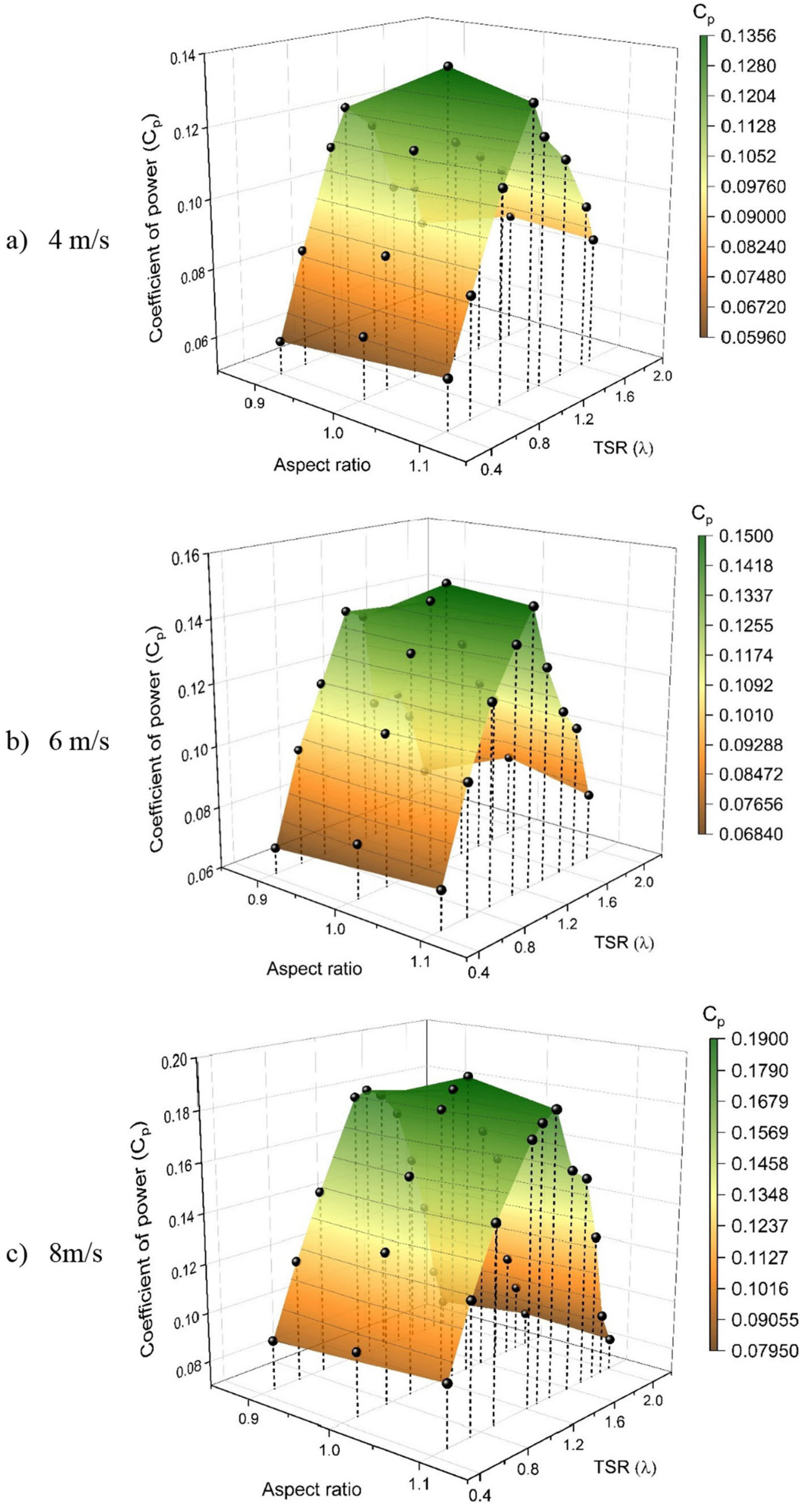

Fig. 11 Coefficient power (C_p) variation of auxiliary H-rotor with various aspect ratio at various wind speeds

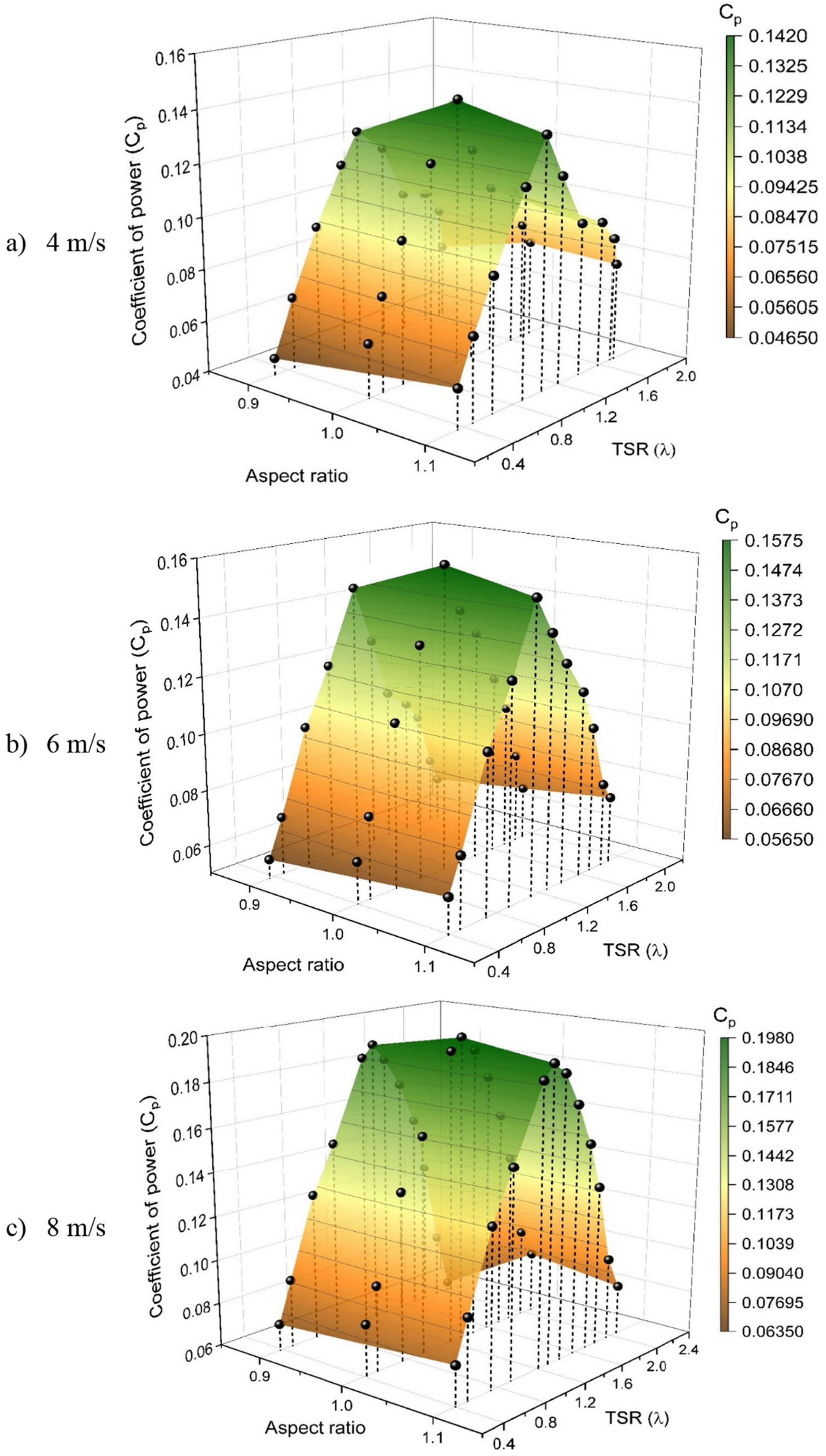
a) 4 m/s

b) 6 m/s

c) 8 m/s

Table 5 Maximum C_p Values of the H-rotors

Wind speed (in m/s)	Aspect ratio	Standard H-rotor		Auxiliary H-rotor		Variation in C_p
		Maximum C_p	TSR	Maximum C_p	TSR	
4	0.9	0.12160	0.95	0.12544	0.98	3%
	1.0	0.13560	1.13	0.14200	1.10	4.7%
	1.1	0.12980	1.10	0.13545	1.05	4.3%
6	0.9	0.13820	1.08	0.14520	1.10	5%
	1.0	0.14994	1.26	0.15732	1.14	4.9%
	1.1	0.14750	1.25	0.15120	1.12	2.5%
8	0.9	0.18070	1.30	0.18963	1.29	5%
	1.0	0.18995	1.45	0.19800	1.32	4.2%
	1.1	0.18318	1.42	0.19257	1.31	5.1%

decrease in C_p up to 3.5% for the standard H-rotor and 3% for the auxiliary H-rotor. At lower wind speeds (4 m/s), altering the aspect ratio from 0.9 to 1.0 results in a significant increase in C_p up to 11.5% for the standard H-rotor and 13% for the auxiliary H-rotor, whereas altering the aspect ratio from 1.0 to 1.1 results in a decrease in C_p up to 4% for the standard H-rotor and 5% for the auxiliary H-rotor. These findings suggest that altering the aspect ratio has a more significant impact on C_p at lower wind speeds. At higher wind speeds, the effect of changing the aspect ratio is relatively minimal. The reason for obtaining the maximum C_p at aspect ratio 1.0 is due to the optimal harvesting of incoming wind energy. At this aspect ratio, the maximum amount of incoming wind is effectively captured and converted into useful energy, while other aspect ratios fail to achieve this. In the case of an aspect ratio of 1.1, the rotor diameter is smaller than the height of the blades, which creates the possibility of poor spinning stability during rotation. This can lead to a decrease in the performance of the H-rotor. In contrast, with an aspect ratio of 0.90, the rotor diameter is larger than the blade height, which causes an increase in the blade-to-blade gap. Consequently, incoming wind can escape from the gap without striking the blades, resulting in the least amount of wind being converted into useful energy [54, 57].

The maximum C_p values (and corresponding TSR values) of the standard and auxiliary H-rotor with different aspect ratios at every applied wind speed are shown in Table 5. It can be observed from Table 5 that the C_p values are superior for the auxiliary H-rotor compared to the standard H-rotor at each applied wind speed. The superior results of the auxiliary H-rotor were associated with two reasons [7, 44, 47]; (i) In the presence of auxiliary airfoils in front of the main airfoil can split the frontal area of the H-rotor, which can lead to extracting more energy from the wind. (ii) Auxiliary airfoils help to separate shear layers from reattaching to the main airfoil so that the lift-drag ratio of the main airfoil blade will improve. As a result, incorporating an auxiliary airfoil into the H-rotor design will improve performance.

5 Conclusions

In this study, how the altering aspect ratio and adding auxiliary blades influence the performance quantities of the H-rotor is examined. For that, the standard H-rotor and auxiliary H-rotor are fabricated for laboratory wind tunnel experiments. The most characteristic feature of fabricated rotors is altering the aspect ratio by changing the diameter of the rotor with the help of a special arrangement. A set of wind tunnel tests are conducted on both the H-rotors, and the following conclusion were drawn from the experimental outcomes.

(a) The aspect ratio of the H-rotor has a considerable effect on the starting behaviour and power output in all tested wind conditions. The experimental outcomes revealed that a well-maintained aspect ratio (height of rotor blade = diameter of the rotor) is a promising option for improving H-rotor's performance. In the present study, both H-rotors with an aspect ratio of 1.0 are exhibited superior performance values than other tested aspect ratios (0.9 and 1.1).

(b) Concerning the static torque, the standard and auxiliary H-rotor exhibit positive static torque values at all tested conditions. However, the auxiliary H-rotor possesses a remarkable static torque coefficient, approximately 81% higher as compared to the standard H-rotor, which shows the auxiliary airfoil has significant advantages in self-starting improvement.

(c) Concerning the dynamic torque, the dynamic toque values are linearly decreased as increasing the TSR for both H-rotor in all tested conditions. However, the standard H-rotor exhibited substantially zero torque at $0.4 < \text{TSR} > 1.9$ values, whereas the auxiliary H-rotor exhibited positive torque at TSR = 0.35 and 2.2, which signifies the auxiliary H-rotor is reliable work in different TSR values.

(d) The study concludes that the maximum C_p values of the modified H-rotor are consistently higher than the standard H-rotor across all tested wind conditions and aspect ratios. Changing the aspect ratio from 0.9 to 1.0 increases C_p values for both types of H-rotors, while changing it from 1.0 to 1.1 decreases C_p values for both types of H-rotors. These results indicate that adding an auxiliary airfoil to an H-rotor can greatly enhance its power performance, especially when paired with an optimal aspect ratio of 1.0.

To advancement of the current work, a numerical simulation can be conducted to fully comprehend the flow phenomena between the main and auxiliary rotor blades. Secondly, though the starting torque seems effective, the improvements in the C_t and C_p values were insignificant. Thus, further experimental research can be carried out on an unsymmetrical airfoil, where effective changes in C_t and C_p values could be observed. Additionally, study the effects of S_l and S_r on the performance of the auxiliary H-rotor, and findings the its optimal distances could the potential avenues for future research of the auxiliary H-rotor.

Acknowledgements The first author would like to sincerely thank the Department of Mechanical Engineering, NIT Silchar, India, for providing experimental facilities.

Author Contributions KUR: Conceptualization, Data curation, Formal analysis, Investigation, Methodology, writing original draft, BD: Conceptualization, Methodology, Resources, Supervision, Writing—review and editing. BR: Conceptualization, Methodology and formal analysis.

Funding No funding is received for this research.

Data Availability Not applicable.

Declarations

Conflict of interest The authors have no conflicts of interest to declare that are relevant to the content of this article.

References

1. Patil, R.; Daróczy, L.; Janiga, G.; Thévenin, D.: Large eddy simulation of an H-Darrieus rotor. Energy **160**, 388–398 (2018). https://doi.org/10.1016/j.energy.2018.06.203
2. Ray, P.: Renewable energy and sustainability. Clean Technol. Environ. Policy. **21**, 1517–1533 (2019). https://doi.org/10.1007/s10098-019-01739-4
3. Bianchini, A.; Balduzzi, F.; Ferrara, G.; Ferrari, L.: Energy-yield-based optimization of a H-Darrieus wind turbine in skewed flow. In: Battisti, L.; Ricci, M. (Eds.) Wind energy exploitation in urban environment, pp. 165–188. Springer, Cham (2018)
4. Hand, B.; Cashman, A.: A review on the historical development of the lift-type vertical axis wind turbine: from onshore to offshore floating application. Sustain. Energy Technol. Assess. (2020). https://doi.org/10.1016/j.seta.2020.100646
5. Tasneem, Z.; Al Noman, A.; Das, S.K.; Saha, D.K.; Islam, M.R.; Ali, F.; Badal, F.; Ahamed, H.; Moyeen, S.I.; Alam, F.: An analytical review on the evaluation of wind resource and wind turbine for urban application: prospect and challenges. Dev. Built Environ. (2020). https://doi.org/10.1016/j.dibe.2020.100033
6. Kothe, L.B.; Möller, S.V.; Petry, A.P.: Numerical and experimental study of a helical Savonius wind turbine and a comparison with a two-stage Savonius turbine. Renew. Energy. **148**, 627–638 (2020). https://doi.org/10.1016/j.renene.2019.10.151
7. Arpino, F.; Scungio, M.; Cortellessa, G.: Numerical performance assessment of an innovative Darrieus-style vertical axis wind turbine with auxiliary straight blades. Energy Convers. Manag. **171**, 769–777 (2018). https://doi.org/10.1016/j.enconman.2018.06.028
8. Du, L.; Ingram, G.; Dominy, R.G.: Experimental study of the effects of turbine solidity, blade profile, pitch angle, surface roughness, and aspect ratio on the H-Darrieus wind turbine self-starting and overall performance. Energy Sci. Eng. **7**, 2421–2436 (2019). https://doi.org/10.1002/ese3.430
9. Mohamed, O.S.; Ibrahim, A.A.; Etman, A.K.; Abdelfatah, A.A.; Elbaz, A.M.R.: Numerical investigation of Darrieus wind turbine with slotted airfoil blades. Energy Convers. Manag. X. **5**, 100026 (2020). https://doi.org/10.1016/j.ecmx.2019.100026
10. Pinheiro, K.A.; de Custódio Filho, S.S.; Vaz, J.R.P.; Mesquita, A.L.A.: Effect of bearing dissipative torques on the dynamic behavior of H-Darrieus wind turbines. J. Braz. Soc. Mech. Sci. Eng. (2021). https://doi.org/10.1007/s40430-021-03122-1
11. Sengupta, A.R.; Biswas, A.; Gupta, R.: Studies of some high solidity symmetrical and unsymmetrical blade H-Darrieus rotors with respect to starting characteristics, dynamic performances and flow physics in low wind streams. Renew. Energy. **93**, 536–547 (2016). https://doi.org/10.1016/j.renene.2016.03.029
12. Untaroiu, A.; Wood, H.G.; Allaire, P.E.; Ribando, R.J.: Investigation of self-starting capability of vertical axis wind turbines using a computational fluid dynamics approach. J. Sol. Energy Eng. Trans. ASME. **133**, 1–8 (2011). https://doi.org/10.1115/1.4004705
13. Arab, A.; Javadi, M.; Anbarsooz, M.; Moghiman, M.: A numerical study on the aerodynamic performance and the self-starting characteristics of a Darrieus wind turbine considering its moment of inertia. Renew. Energy. **107**, 298–311 (2017). https://doi.org/10.1016/j.renene.2017.02.013
14. Zhu, J.; Huang, H.; Shen, H.: Self-starting aerodynamics analysis of vertical axis wind turbine. Adv. Mech. Eng. **7**, 1–12 (2015). https://doi.org/10.1177/1687814015620968
15. Zamani, M.; Sangtarash, A.; Javad Maghrebi, M.: Numerical study of porous media effect on the blade surface of vertical axis wind turbine for enhancement of aerodynamic performance. Energy Convers. Manag. **245**, 114598 (2021). https://doi.org/10.1016/j.enconman.2021.114598
16. Li, Q.; Maeda, T.; Kamada, Y.; Shimizu, K.; Ogasawara, T.; Nakai, A.; Kasuya, T.: Effect of rotor aspect ratio and solidity on a straight-bladed vertical axis wind turbine in three-dimensional analysis by the panel method. Energy **121**, 1–9 (2017). https://doi.org/10.1016/j.energy.2016.12.112
17. Belabes, B.; Paraschivoiu, M.: Numerical study of the effect of turbulence intensity on VAWT performance. Energy **233**, 121139 (2021). https://doi.org/10.1016/j.energy.2021.121139
18. Satrio, D.; Utama, I.K.A.P.: Experimental investigation into the improvement of self-starting capability of vertical-axis tidal current turbine. Energy Rep. **7**, 4587–4594 (2021). https://doi.org/10.1016/j.egyr.2021.07.027
19. Mazarbhuiya, H.M.S.M.; Biswas, A.; Sharma, K.K.: Blade thickness effect on the aerodynamic performance of an asymmetric

NACA six series blade vertical axis wind turbine in low wind speed. Int. J. Green Energy. **17**, 171–179 (2020). https://doi.org/10.1080/15435075.2020.1712214
20. Zhang, T.; Wang, Z.; Huang, W.; Ingham, D.; Ma, L.; Pourkashanian, M.: A numerical study on choosing the best configuration of the blade for vertical axis wind turbines. J. Wind Eng. Ind. Aerodyn. **201**, 104162 (2020). https://doi.org/10.1016/j.jweia.2020.104162
21. Ghiasi, P.; Najafi, G.; Ghobadian, B.; Jafari, A.; Mazlan, M.: Analytical study of the impact of solidity, chord length, number of blades, aspect ratio and airfoil type on H-rotor Darrieus wind turbine performance at low reynolds number. Sustain. (2022). https://doi.org/10.3390/su14052623
22. Peng, H.Y.; Lam, H.F.; Liu, H.J.: Power performance assessment of H-rotor vertical axis wind turbines with different aspect ratios in turbulent flows via experiments. Energy **173**, 121–132 (2019). https://doi.org/10.1016/j.energy.2019.01.140
23. Song, C.; Wu, G.; Zhu, W.; Zhang, X.: Study on aerodynamic characteristics of darrieus vertical axis wind turbines with different airfoil maximum thicknesses through computational fluid dynamics. Arab. J. Sci. Eng. **45**, 689–698 (2020). https://doi.org/10.1007/s13369-019-04127-8
24. Nguyen, C.C.; Le, H.H.; Chi, H.; Le, T.H.H.; Tran, P.T.: A numerical study of thickness effect of the symmetric NACA 4 digit airfoils on self starting capability of a 1kW H-type vertical axis wind turbine. Int. J. Mech. Eng. Appl. Spec. Issue Transp. Eng. Technol. **3**, 7–16 (2015). https://doi.org/10.11648/j.ijmea.s.2015030301.12
25. Parker, C.M.; Leftwich, M.C.: The effect of tip speed ratio on a vertical axis wind turbine at high Reynolds numbers. Exp. Fluids. **57**, 1–11 (2016). https://doi.org/10.1007/s00348-016-2155-3
26. Jain, S.; Saha, U.K.: On the influence of blade thickness-to-chord ratio on dynamic stall phenomenon in H-type Darrieus wind rotors. Energy Convers. Manag. **218**, 113024 (2020). https://doi.org/10.1016/j.enconman.2020.113024
27. Sreejith, B.K.; Sathyabhama, A.: Experimental and numerical study of laminar separation bubble formation on low Reynolds number airfoil with leading-edge tubercles. J. Braz. Soc. Mech. Sci. Eng. **42**, 1–15 (2020). https://doi.org/10.1007/s40430-020-2229-2
28. Sobhani, E.; Ghaffari, M.; Maghrebi, M.J.: Numerical investigation of dimple effects on darrieus vertical axis wind turbine. Energy **133**, 231–241 (2017). https://doi.org/10.1016/j.energy.2017.05.105
29. Ni, L.; Miao, W.; Li, C.; Liu, Q.: Impacts of Gurney flap and solidity on the aerodynamic performance of vertical axis wind turbines in array configurations. Energy **215**, 118915 (2021). https://doi.org/10.1016/j.energy.2020.118915
30. Bianchini, A.; Balduzzi, F.; Di Rosa, D.; Ferrara, G.: On the use of Gurney Flaps for the aerodynamic performance augmentation of Darrieus wind turbines. Energy Convers. Manag. **184**, 402–415 (2019). https://doi.org/10.1016/j.enconman.2019.01.068
31. Dessoky, A.; Bangga, G.; Lutz, T.; Krämer, E.: Aerodynamic and aeroacoustic performance assessment of H-rotor darrieus VAWT equipped with wind-lens technology. Energy **175**, 76–97 (2019). https://doi.org/10.1016/j.energy.2019.03.066
32. Zidane, I.F.; Ali, H.M.; Swadener, G.; Eldrainy, Y.A.; Shehata, A.I.: Effect of upstream deflector utilization on H-Darrieus wind turbine performance : an optimization study. Alex. Eng. J. (2022). https://doi.org/10.1016/j.aej.2022.07.052
33. Yousefi Roshan, M.; Khaleghinia, J.; Eshagh Nimvari, M.; Salarian, H.: Performance improvement of Darrieus wind turbine using different cavity layouts. Energy Convers. Manag. **246**, 114693 (2021). https://doi.org/10.1016/j.enconman.2021.114693
34. Syawitri, T.P.; Yao, Y.; Yao, J.; Chandra, B.: Geometry optimisation of vertical axis wind turbine with Gurney flap for performance enhancement at low, medium and high ranges of tip speed ratios. Sustain. Energy Technol. Assessments. **49**, 101779 (2022). https://doi.org/10.1016/j.seta.2021.101779
35. Zhu, H.; Hao, W.; Li, C.; Luo, S.; Liu, Q.; Gao, C.: Effect of geometric parameters of Gurney flap on performance enhancement of straight-bladed vertical axis wind turbine. Renew. Energy. **165**, 464–480 (2021). https://doi.org/10.1016/j.renene.2020.11.027
36. Liu, Q.; Miao, W.; Ye, Q.; Li, C.: Performance assessment of an innovative Gurney flap for straight-bladed vertical axis wind turbine. Renew. Energy. **185**, 1124–1138 (2022). https://doi.org/10.1016/j.renene.2021.12.098
37. Wang, Z.; Zhuang, M.: Leading-edge serrations for performance improvement on a vertical-axis wind turbine at low tip-speed-ratios. Appl. Energy. **208**, 1184–1197 (2017). https://doi.org/10.1016/j.apenergy.2017.09.034
38. Yan, Y.; Avital, E.; Williams, J.; Cui, J.: Aerodynamic performance improvements of a vertical axis wind turbine by leading-edge protuberance. J. Wind Eng. Ind. Aerodyn. **211**, 104535 (2021). https://doi.org/10.1016/j.jweia.2021.104535
39. Lositaño, I.C.M.; Danao, L.A.M.: Steady wind performance of a 5 kW three-bladed H-rotor Darrieus Vertical Axis Wind Turbine (VAWT) with cambered tubercle leading edge (TLE) blades. Energy **175**, 278–291 (2019). https://doi.org/10.1016/j.energy.2019.03.033
40. Gonçalves, A.N.C.; Pereira, J.M.C.; Sousa, J.M.M.: Passive control of dynamic stall in a H-Darrieus vertical axis wind turbine using blade leading-edge protuberances. Appl. Energy. **324**, 119700 (2022). https://doi.org/10.1016/j.apenergy.2022.119700
41. Zamani, M.; Maghrebi, M.J.; Varedi, S.R.: Starting torque improvement using J-shaped straight-bladed Darrieus vertical axis wind turbine by means of numerical simulation. Renew. Energy. **95**, 109–126 (2016). https://doi.org/10.1016/j.renene.2016.03.069
42. Chen, J.; Yang, H.; Yang, M.; Xu, H.: The effect of the opening ratio and location on the performance of a novel vertical axis Darrieus turbine. Energy **89**, 819–834 (2015). https://doi.org/10.1016/j.energy.2015.05.136
43. Li, S.; Li, Y.; Yang, C.; Wang, Q.; Zhao, B.; Li, D.; Zhao, R.; Ren, T.; Zheng, X.; Gao, Z.; Xu, W.: Experimental investigation of solidity and other characteristics on dual vertical axis wind turbines in an urban environment. Energy Convers. Manag. (2021). https://doi.org/10.1016/j.enconman.2020.113689
44. Scungio, M.; Arpino, F.; Focanti, V.; Profili, M.; Rotondi, M.: Wind tunnel testing of scaled models of a newly developed Darrieus-style vertical axis wind turbine with auxiliary straight blades. Energy Convers. Manag. **130**, 60–70 (2016). https://doi.org/10.1016/j.enconman.2016.10.033
45. Asr, M.T.; Nezhad, E.Z.; Mustapha, F.; Wiriadidjaja, S.: Study on start-up characteristics of H-Darrieus vertical axis wind turbines comprising NACA 4-digit series blade airfoils. Energy **112**, 528–537 (2016). https://doi.org/10.1016/j.energy.2016.06.059
46. Uma Reddy, K.; Deb, B.; Roy, B.; Rashid, S.M.: Flow physics analysis on the effect of cambered airfoil blades on vertical axis wind turbines using CFD. Lect. Notes Mech. Eng. (2020). https://doi.org/10.1007/978-981-32-9931-3_55
47. Li, Y.; Zhao, C.; Qu, C.; Zhao, S.; Feng, F.; Tagawa, K.: Effect of auxiliary blade on aerodynamic characteristics of vertical axis wind turbine by numerical simulation. Int. J. Rotating Mach. (2019). https://doi.org/10.1155/2019/8098160
48. Yagmur, S.; Kose, F.: Numerical evolution of unsteady wake characteristics of H-type Darrieus hydrokinetic turbine for a hydro farm arrangement. Appl. Ocean Res. **110**, 102582 (2021). https://doi.org/10.1016/j.apor.2021.102582
49. Bundi, J.M.; Ban, X.; Wekesa, D.W.; Ding, S.: Pitch control of small H-type Darrieus vertical axis wind turbines using advanced gain scheduling techniques. Renew. Energy. **161**, 756–765 (2020). https://doi.org/10.1016/j.renene.2020.05.184
50. Singh, M.A.; Biswas, A.; Misra, R.D.: Investigation of self-starting and high rotor solidity on the performance of a three S1210 blade

H-type Darrieus rotor. Renew. Energy. **76**, 381–387 (2015). https://doi.org/10.1016/j.renene.2014.11.027

51. Mazarbhuiya, H.M.S.M.; Biswas, A.; Sharma, K.K.: Effect of blade attachments on the performance of an asymmetric blade H-Darrieus turbine at low wind speed. Energy Sources Part A Recover. Util. Environ. Eff. (2020). https://doi.org/10.1080/15567036.2020.1826601
52. Mishra, N.; Gupta, A.S.; Dawar, J.; Kumar, A.; Mitra, S.: Numerical and experimental study on performance enhancement of Darrieus vertical axis wind turbine with wingtip devices. J. Energy Resour. Technol. (2018). https://doi.org/10.1115/1.4040506
53. Babadi Soultanzadeh, M.; Moradi, A.: Numerical simulation and experimental study of blade pitch effect on Darrieus straight-bladed wind turbine with high solidity. SN Appl. Sci. **3**, 1–13 (2021). https://doi.org/10.1007/s42452-021-04465-z
54. Uma Reddy, K.; Deb, B.; Roy, B.: A numerical and experimental study on the performance of a conventional H- Darrieus wind rotor with auxiliary blades. Ocean Eng. **280**, 114697 (2023). https://doi.org/10.1016/j.oceaneng.2023.114697
55. Li, Y.; Zheng, Y.F.; Feng, F.; He, Q.B.; Wang, N.X.: Numerical simulation on a straight-bladed vertical axis wind turbine with auxiliary blade. IOP Conf. Ser. Earth Environ. Sci. (2016). https://doi.org/10.1088/1755-1315/40/1/012062
56. Roy, S.; Das, R.; Saha, U.K.: An inverse method for optimization of geometric parameters of a Savonius-style wind turbine. Energy Convers. Manag. **155**, 116–127 (2018). https://doi.org/10.1016/J.ENCONMAN.2017.10.088
57. Naccache, G.; Paraschivoiu, M.: Development of the dual vertical axis wind turbine using computational fluid dynamics. J. Fluids Eng. Trans. (2017). https://doi.org/10.1115/1.4037490